Available online at www.sciencedirect.com

ScienceDirect

Polar Science 8 (2014) 10–23

http://ees.elsevier.com/polar/

Comparison of tide model outputs for the northern region of the Antarctic Peninsula using satellite altimeters and tide gauge data

Fernando A. Oreiro [a,b,*], Enrique D'Onofrio [a,b], Walter Grismeyer [a], Mónica Fiore [a,b], Martín Saraceno [c,d,e]

[a] *Servicio de Hidrografía Naval, Ministerio de Defensa, Av. Montes de Oca 2124 (C1270ABV), Ciudad Autónoma de Buenos Aires, Argentina*
[b] *Instituto de Geodesia y Geofísica Aplicadas, Universidad de Buenos Aires, Argentina*
[c] *Centro de Investigaciones del Mar y la Atmosfera (CONICET), Argentina*
[d] *Departamento de Ciencias de la Atmósfera y los Océanos, Universidad de Buenos Aires, Argentina*
[e] *Instituto Franco-Argentino de Estudios sobre el Clima y sus Impactos (IFAECI, CNRS/CONICET-UBA), Argentina*

Received 5 July 2013; revised 18 October 2013; accepted 2 December 2013
Available online 11 December 2013

Abstract

This study compares the common harmonic constants of the O_1, K_1, P_1, Q_1, M_2, S_2, N_2, and K_2 tidal constituents from eight global and four regional tide models with harmonic constants from satellite altimeter and tide gauge data for the northern region of the Antarctic Peninsula (58°S–66°S, 53°W–66°W). To obtain a more representative comparison, the study area was divided into three zones with different physical characteristics but similar maximum tidal amplitude variations: Zone I (north of 62°S), Zone II (south of 62°S and west of the Antarctic Peninsula), and Zone III (between 62°S and 64.3°S, and east of 58.5°W). Root sum square (RSS) values are less than or equal to 3.0, 4.2, and 8.4 cm for zones I, II, and III, respectively. No single model shows superior performance in all zones. Because there are insufficient satellite altimetry observations in the vicinity of Matienzo Base (64.9761°S, 60.0683°W), this station was analyzed separately and presents the greatest values of both root mean square misfit and RSS. The maximum, minimum, and average amplitude values of the constituents that follow in importance after the eight common tidal constituents, and which have amplitudes greater than 1 cm, are also analyzed.

Keywords: Sea-surface height; Tide modeling; Antarctic Peninsula; Coastal satellite altimetry

1. Introduction

Knowledge of tides not only contributes to many practical applications in the marine environment, such as navigation and contaminant-dispersion modeling, but is also important in a wide range of scientific studies. For example, microstructure studies have shown a correlation between the rate of turbulent dissipation and tide cycles (Polzin et al., 1997; Ledwell et al., 2000), and there is increasing evidence that tides may provide a significant source of energy for the mixing that takes place in the deep ocean (Munk and Wunsch, 1998; Egbert and Ray, 2000, 2001). At the coast, the tide contributes significantly to vertical

* Corresponding author. Servicio de Hidrografía Naval, Ministerio de Defensa, Av. Montes de Oca 2124 (C1270ABV), Ciudad Autónoma de Buenos Aires, Argentina. Tel.: +54 11 58421558.
E-mail addresses: mareas@hidro.gov.ar, foreiro@hidro.gov.ar (F. A. Oreiro).

1873-9652/$ - see front matter © 2013 Elsevier B.V. and NIPR. All rights reserved.
http://dx.doi.org/10.1016/j.polar.2013.12.001

mixing, redistributing nutrients and oxygen and therefore influencing marine life (Romero et al., 2006), and to CO_2 exchange between ocean and atmosphere (Bianchi et al., 2005). In the Antarctic Ocean, tides interact with the floating ice sheet (Legrésy et al., 2004; Brunt et al., 2010), influence the ice-sheet grounding zone, modify sea-ice formation in front of ice shelves, and probably also play a role in iceberg formation (King et al., 2011).

In some studies, the tidal signal is regarded as noise and must therefore be removed. This is the case for satellite measurements of ice-shelf-surface height (laser altimetry) and ice motion (Interferometric Synthetic Aperture Radar, inSAR), where tides are the primary cause of the time-dependent ice-shelf-height signal, which requires accurate removal of the tidal signal (Padman et al., 2001). For fixed stations, such as mooring sites, it is possible to remove the tide using numerical filters. Because of the sampling rate of satellites, the signal retrieved can be affected by aliasing. Aliasing refers to the effect whereby different signals become indistinguishable (or aliases of one another) when sampled. It also refers to the distortion that results when the signal reconstructed from samples differs from the original continuous signal. According to the Nyquist criterion, aliasing occurs when the variability in a signal occurs at scales smaller than twice the sampling interval (Bendat and Piersol, 1971). A direct consequence of the aliasing effect is that short-scale signals may appear in the measurements at longer or even infinite scales (Chen and Lin, 2000). Thus, direct filtering is not feasible and requires the use of both global and regional models.

During the past 20 years, the accuracy of such global and regional models has been improved. However, model results in Antarctica and near coasts are less accurate than in the rest of the ocean (Padman et al., 2002; Lyard et al., 2006). Several reasons may account for this lack of accuracy, such as bathymetric uncertainties, the quality and amount of tidal data assimilated into the models, and an inadequate number of tidal constituents. Furthermore, the limited availability of direct tide observations in Antarctica (see http://www.psmsl.org/products/data_coverage/) indicates the need for ongoing research on this topic. Although there is a history of reports of direct tide observations in the Antarctic region (Lutjeharms et al., 1985; Pedley et al., 1986; Foldvik et al., 1990; Levine et al., 1997), these have limited spatial coverage. Since the launch of the Topex–Poseidon mission in 1992, spatial coverage has improved; however, satellite altimeter measurements at high latitudes are scarcer than in other regions of the ocean, due to ice coverage during most of the year. With more than 20 years of data now available, the number of altimetry observations in Antarctica has allowed the precise harmonic constants of tide to be obtained in certain regions.

The aim of this work is to compare harmonic constants from 12 of the most up-to-date global and regional tide models with harmonic constants from satellite altimeter and tide gauge data for the northern region of the Antarctic Peninsula (58°S–66°S, 53°W–66°W; Fig. 1). An evaluation of the performance of tide models in this area will contribute to the development of more accurate results in oceanographic and climatic studies. In addition, tide models can be used to detide altimetry data in order to compute large-scale patterns of sea-surface height (SSH) and associated geostrophic velocities (e.g., Saraceno et al., 2010).

A new harmonic analysis methodology is implemented that allows the use of sea-level heights with missing data and uneven sampling intervals. Time series from 20 coastal tide gauges are used; 3 of these series are longer than six years, 13 are longer than a month, and 4 are longer than a fortnight.

2. Tide gauge records and model output

2.1. Tide gauge records

In the Antarctic Peninsula, tide observations have been conducted mainly in the vicinity of the scientific bases located in the northwestern part of the Antarctic Peninsula (Fig. 1). These observations were made using float tide gauges, water-level recorders with pressure sensors, and tide poles. Table 1 presents information for the time series analyzed for each tide station, including latitude, longitude, period, length in days, and type of measuring device. The full record available at each station was used, despite missing data in some cases, because a longer series allows more precise harmonic constants to be calculated. All data used were obtained by the Argentine Naval Hydrographic Service, apart from those measured by the Hydrographic and Oceanographic Service of the Chilean Navy in Arturo Prat Base. Measurements made with float tide gauges and pressure sensors were performed according to the standards of the Argentine Naval Hydrographic Service, with an error of ±1 cm, whereas for tide poles the error is ±3 cm. According to the University of Hawaii Sea Level Center, Prat Base data appear to be of good quality (ftp://ilikai.soest.hawaii.edu/rqds/atlantic/doc/qa730a.dmt).

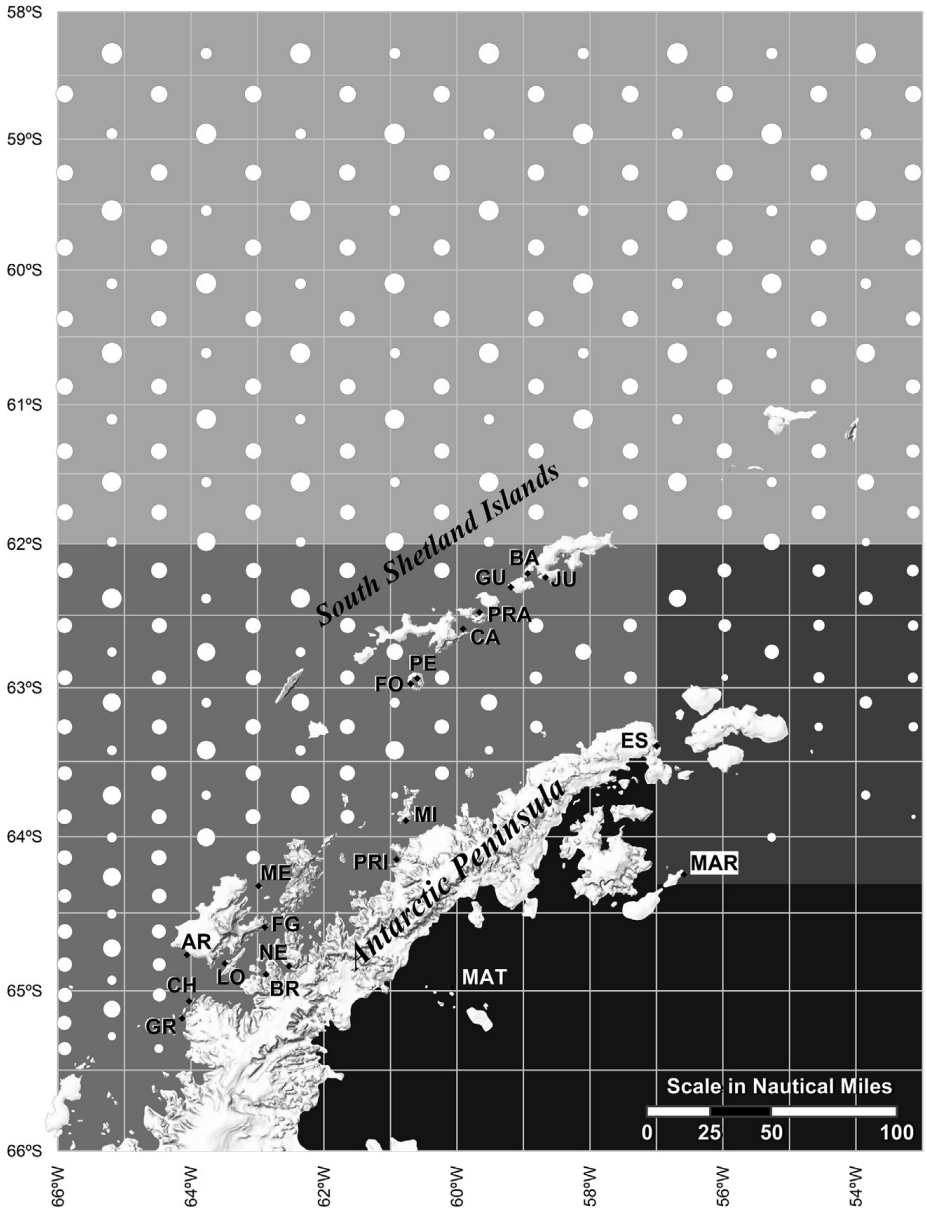

Fig. 1. Cartographic representation of the study area. Tide stations are indicated with up to three characters; full name and coordinates are given in Table 1. Altimetry data are shown with a circle whose size is proportional to the number of SSH data. The study area is divided into three zones for calculating the RMS misfit and RSS. Zones I, II, and III are marked in light, medium, and dark gray, respectively.

2.2. Satellite altimeter measurements

The Corrected SSHs (CorSSHs) were produced by Collecte Localisation Satellites (CLS) Space Oceanography Division and distributed by Archiving, Validation and Interpretation of Satellite Oceanographic data (AVISO), with support from the Centre National d'Etudes Spatiales (CNES). Data from TOPEX/Poseidon and the Jason-1 and Jason-2 altimeters were used for the period October 1992 to January 2012 (ftp://ftp.aviso.oceanobs.com/pub/oceano/AVISO/SSH/monomission/dt/corssh/ref/). Because the study area is located at the northernmost extremity of the Antarctic continent, where climatic conditions are extreme and for a large part of the year ice covers the surface, few locations yield useful altimetry observations. Cross-track areas gather unevenly spaced data within the same cycle and, consequently, a larger number of sea-level observations. For this reason, crossover points are evaluated in this study. The cross-track variations in altimeter satellite ground-tracks are maintained within 1 km of the nominal ground track (Chelton et al., 2001). Sea-level data were gathered using circles of 2.5-km radius centered at the

Table 1
List of locations where sea level was measured, period of measurement, duration of each sea-level record (in days), and type of device used. Codes in parentheses in the first column refer to locations in Fig. 1. TP: Tide Pole; F: Floater; P: Pressure Sensor. The asterisk (*) indicates the use of the Rayleigh criterion to decontaminate and infer harmonic constants.

Station (Code)	Latitude (°)	Longitude (°)	Period	Days	Type of device
Balveé Refuge (BA)*	−62.2092	−58.9353	05/01/1954–18/02/1954	44	TP
Carlini Base, ex Jubany (JU)*	−62.2371	−58.6676	01/01/1988–09/02/1988	40	P
Gurruchaga Refuge (GU)*	−62.3055	−59.1919	03/01/1958–12/02/1958	41	TP
Arturo Prat Base (PRA)	−62.4833	−59.6333	08/03/1984–31/12/2002	6587	P
Cámara Base (CA)*	−62.5950	−59.9061	06/01/1989–15/02/1989	38	F
Caleta Pendulo Refuge (PE)*	−62.9167	−60.6000	01/02/1955–19/02/1955	53	TP
Port Foster (FO)*	−62.9738	−60.6969	05/01/1958–07/02/1958	33	TP
Esperanza Base (ES)	−63.3955	−56.9944	16/01/1969–31/10/1978	2416	F
Mikkelsen Port (MI)*	−63.8951	−60.7700	07/01/1955–31/01/1955	25	TP
Primavera Base (PRI)*	−64.1515	−60.9106	22/02/1954–22/01/1958	180	TP
Marambio Island (MAR)*	−64.2511	−56.5857	27/01/2001–28/02/2001	32	TP
Port Melchior (ME)*	−64.3243	−62.9822	02/01/1956–04/02/1956	33	TP
Gerlache Mooring (FG)*	−64.5931	−62.8900	17/01/1991–14/02/1991	29	P
Port Arturo (AR)*	−64.7703	−64.0595	08/01/1992–07/02/1992	30	P
Port Lockroy (LO)*	−64.8257	−63.4926	23/01/1992–11/02/1992	19	F
Port Neko (NE)*	−64.8428	−62.5269	07/03/1949–06/04/1949	31	TP
Brown Base (BR)	−64.8953	−62.8713	01/01/1970–01/03/1991	3676	F
Matienzo Base (MAT)*	−64.9761	−60.0683	20/12/1996–21/01/1997	31	P
Port Charcot (CH)*	−65.0651	−64.0285	29/12/1956–24/02/1957	58	TP
Groussac Refuge (GR)*	−65.1754	−64.1354	27/12/1956–23/02/1957	59	TP

intersections of satellite tracks. Dragani et al. (2005) have shown that the tidal wave propagates very rapidly, reaching a height variation of 3 mm in a circle of 2.5-km radius within the study area. Therefore, the tidal variation is significantly smaller than the 3–5-cm approximate precision of TOPEX/Jason (Chelton et al., 2001; Yi et al., 2006; Birkett et al., 2011).

The ocean-tide correction, provided in the CorSSH files, was added to the CorSSH data without modifying the rest of the corrections required for such data. A total of 293 possible altimetry series that could be used to calculate the tidal harmonic constants were obtained. Taking into account the sampling interval of 9.9156 days (Chelton et al., 2001) and the number of

Table 2
Main properties of the tide models used for comparison.

Model	Resolution	Constituents			
		Diurnal	Semidiurnal	Shallow water	Long-period
Global models					
GOT4.7	1/2° × 1/2°	K_1, O_1, P_1, Q_1, S_1	M_2, S_2, N_2, K_2	M_4	
TPXO7.2	1/4° × 1/4°	K_1, O_1, P_1, Q_1	M_2, S_2, N_2, K_2	M_4, MS_4, MN_4	M_m, M_f
TPXO8	1/6° × 1/6°			MS_4, MN_4	M_m, M_f
	1/30° × 1/30°	K_1, O_1, P_1, Q_1	M_2, S_2, N_2, K_2	M_4	
FES2004	1/8° × 1/8°	K_1, O_1, P_1, Q_1, S_1	M_2, S_2, N_2, K_2, $2N_2$,	M_4	M_m, M_f, M_{tm}, M_{sqm}
FES2012	1/16° × 1/16°	K_1, O_1, P_1, Q_1, S_1, J_1	M_2, S_2, N_2, K_2, $2N_2$, E_2, MKS_2, T_2, La_2, R_2, Nu_2, L_2, Mu_2	M_3, M_4, MN_4, N_4, MS_4, S_4, M_6, M_8	S_{sa}, M_m, M_{tm}, M_f, MS_f
EOT10a	1/8° × 1/8°	K_1, O_1, P_1, Q_1, S_1	M_2, S_2, N_2, K_2, $2N_2$	M_4	M_m, M_f
EOT11a	1/8° × 1/8°	K_1, O_1, P_1, Q_1, S_1	M_2, S_2, N_2, K_2, $2N_2$	M_4	M_m, M_f
DTU10	1/8° × 1/8°	K_1, O_1, P_1, Q_1, S_1	M_2, S_2, N_2, K_2	M_4	
Regional Models					
AO-ATLAS 2011	1/4° × 1/12°	K_1, O_1, P_1, Q_1	M_2, S_2, N_2, K_2	M_4, MS_4, MN_4	
CADA00.10	1/4° × 1/12°	K_1, O_1, P_1, Q_1	M_2, S_2, N_2, K_2		M_m, M_f
ANTPEN04.01	1/30° × 1/60°	K_1, O_1, P_1, Q_1	M_2, S_2, N_2, K_2		
CATS2008	4-km Node spacing	K_1, O_1, P_1, Q_1	M_2, S_2, N_2, K_2		M_m, M_f

missing data, 232 series were identified as being suitable for applying the methodology explained below in Section 3.1 (Fig. 1). The series with small quantities of data correspond mostly to the southeastern part of the study area (Fig. 1), where there is more permanent and seasonal sea ice.

2.3. Tide models used

Whereas global models have substantially improved knowledge of tides at a global scale, in polar regions and near the coasts they are less accurate than in the rest of the ocean (Padman et al., 2008). This limitation has led to higher-resolution regional applications being developed for specific areas. To understand and adequately predict the tide in Antarctic waters, it is necessary to make careful comparisons of numerical solutions with the corresponding tide gauge and satellite observations.

Harmonic constants obtained from eight global (GOT4.7, TPXO7.2, TPXO8, FES2004, FES2012, EOT10a, EOT11a, and DTU10) and four regional (AO-ATLAS-2011, CADA00.10, ANTPEN04.01, and CATS2008) tide models were used. The global models selected are the most commonly used for eliminating the tidal signal from altimetry measurements. The regional model for the Atlantic Ocean (AO-ATLAS-2011) includes the Antarctic Peninsula, and CATS2008 and CADA00.10 are regional models of the entire circum-Antarctic ocean. ANTPEN04.01 is a regional model of the entire Antarctic Peninsula and does not incorporate observed tidal information. It should be noted that the present study does not attempt to make a complete classification of all the different tide models available. Table 2 presents the resolution and constituents of the 12 tide models used.

The Goddard Ocean Tide (GOT) model GOT4.7 is an update of GOT00, which in turn is an update of GOT99.2 (Ray, 1999). GOT model GOT99.2 is an empirical solution for the amplitudes and phases of the global oceanic tides, based on more than six years of sea-surface height measurements by the TOPEX/Poseidon satellite altimeter. GOT4.7 model solution includes 10 tidal constituents.

The Inverse Tide Model TPXO7.2 was developed at Oregon State University (Egbert and Erofeeva, 2002) and is an update of TPXO7.1. This model solution assimilates tidal data of different satellite missions and in situ tide gauge data and includes 13 tidal constituents. TPXO8 is an update of TPXO7.2 and, unlike the previous inverse tide model solutions, has a high-resolution grid (1/30° × 1/30°) for 9 global constituents and a lower-resolution grid (1/6° × 1/6°) for 4 additional constituents in coastal areas. This model solution, like TPXO7.2, also assimilates tidal data of different satellite missions and in situ tide gauge data, and includes the same 13 tidal constituents.

The finite element solution (FES) tide model FES2004, an update of FES99, is based on nonlinear barotropic shallow-water equations, with bottom friction parameterized through a quadratic dependency on local tidal velocities and through tidal forcing derived from astronomical potential, and includes earth tide, ocean-tide loading, and shelf attraction. This model includes 15 tidal constituents (Lyard et al., 2006) and assimilates tide gauge and satellite data. FES2012 is the latest version of the FES tide model and was developed in 2012. This model uses a new high-resolution global bathymetry and a new global finite element grid. The model includes 32 tidal constituents and assimilates tide gauge and satellite data (Carrère et al., 2012).

The Empirical Ocean Tide (EOT) model EOT10a is an update of EOT08a, developed through the empirical analysis of nearly 18 years of multimission satellite altimeter data. This model includes 13 tidal constituents (Savcenko and Bosch, 2010). Empirical Ocean Tide model EOT11a is another version of the EOT model and was obtained by residual tidal analysis of multimission altimeter data using data from TOPEX/Poseidon, ERS-2, ENVISAT, and Jason-1 and -2. This model includes 13 tidal constituents (Savcenko and Bosch, 2011).

The global empirical ocean tide model of the Technical University of Denmark, DTU10, is based on FES2004 and uses a response method that calculates the relationship between the observed tide at a point and the tidal potential (Munk and Cartwright, 1966). The model uses 17 years of multimission measurements from TOPEX/Poseidon (phases A and B), Jason-1 (phases A and B), and Jason-2 satellite altimetry for sea-level residuals analysis, and includes 10 tidal constituents (Cheng and Andersen, 2011).

The Atlantic Ocean ATLAS (AO-ATLAS) is a regional tide model that covers the Atlantic Ocean, and AO-ATLAS-2011 is the latest version of the 1/12° Atlantic Ocean solution. In coastal areas with complex topographical features, the quality of global and regional solutions is limited by their relatively coarse resolution. ATLAS solutions incorporate existing higher-resolution local solutions into a global or regional solution. The ATLAS solution corresponds to a basic solution in deep water and to local solutions interpolated onto the coarser grid in coastal areas. The model assimilates cycles of TOPEX/Poseidon and

Jason-1 data, cycles of Topex Tandem data in shallow-water and cycles of ERS data in shallow-water and above 66°N. This model includes 11 tidal constituents (http://volkov.oce.orst.edu/tides/atlas.html).

The Circum-Antarctic Tidal Simulation Inverse Model CADA00.10 is a medium-resolution, regional inverse model of the entire circum-Antarctic ocean south of 58°S. The model domain includes ocean cavities under the floating ice shelves. This model assimilates TOPEX/Poseidon satellite altimetry and 25 tide gauge and benthic pressure records from the Antarctic region. The model includes 10 tidal constituents (Padman et al., 2002).

The Antarctic Peninsula High-Resolution Tidal Forward Model ANTPEN04.01 is a regional model of the entire Antarctic Peninsula region. The model domain includes ocean cavities under the floating ice shelves and is based on linearized shallow-water equations, forced at the open boundary by tide heights from the circum-Antarctic forward model (CATS02.01) and by astronomical forcing. This model includes 8 tidal constituents (http://www.esr.org/polar_tide_models/Model_AntPen0401.html).

Circum-Antarctic Tidal Simulation Inverse Model (Version 2008a) CATS2008 is a high-resolution regional model of the entire circum-Antarctic ocean. The model domain includes ocean cavities under the floating ice shelves. This model uses direct factorization of the linearized shallow-water equations, forced at the open boundary by tide heights from the global inverse model TPXO7.1 and by astronomical potentials. It also assimilates TOPEX/Poseidon radar altimetry from the open ocean when no sea ice is present, "high-quality" tide records, and ICESat laser altimetry data at crossovers on the Ross and Filchner-Ronne ice shelves. This model includes 10 tidal constituents (http://www.esr.org/polar_tide_models/Model_CATS2008a.html).

3. Methodology

This section explains the techniques used for the harmonic analysis of tide gauge and satellite altimetry data series, and the procedures used to compare the harmonic constants obtained with those derived from global and regional tide models.

3.1. Harmonic analysis of data

The least squares method was applied to Equation (1) to obtain tidal harmonic constants using tide gauge and satellite data series, as follows:

$$h(t) = Z_0 + \Delta Z \cdot t + \sum_{j=1}^{n} H_j \cdot f_j \cdot \cos\left((V+u)_j - g_j\right) \quad (1)$$

where $h(t)$ is the height of the tide at observation time t, Z_0 is the mean height of the water level at the beginning of the series, ΔZ is the linear trend of the series, H_j is the amplitude of the j constituent, f_j is the nodal factor of the j constituent, $(V+u)_j$ is the value of the equilibrium argument of the j constituent, g_j is the epoch of the j constituent, and n is the number of constituents. The equilibrium argument and the nodal factors were calculated following Cartwright (1985).

Unlike traditional harmonic analysis (Pugh, 1987, 2004; Schureman, 1988), Equation (1) requires the calculation of both the equilibrium argument and nodal factor for each observation time, thus avoiding the use of the speed of the constituent. This is because the angular velocity is defined by the part V of the equilibrium argument and does not consider the temporal variation in the part u (an 18.61-year period). Considering the long length of the series, the mean sea-level linear variation is taken into account through the first two terms of Equation (1).

The common set of harmonic constants of constituents Q_1, O_1, P_1, K_1, N_2, M_2, S_2, and K_2 from 12 global and regional tide models was used for the comparison with harmonic constants from the satellite altimeter and tide gauge data (Table 2). In a data series corresponding to a conventional tide gauge, without missing data, the Rayleigh criterion (Pugh, 1987; Schureman, 1988) is used to infer the minimum time period required to resolve any two tidal frequency constituents in the harmonic analysis. The data sampling rate of the TOPEX and Jason altimeters (9.9156 days) induces aliasing into the frequencies of the tidal constituents. Since these frequencies are known, it is possible to find the corresponding aliasing frequencies (Smith et al., 2000; Chelton et al., 2001) and therefore to continue applying the Rayleigh criterion, provided that the sampling interval remains unchanged. If data are lacking, and/or the time series is taken from the intersection of two tracks, then the sampling interval is variable and it is not possible to apply the Rayleigh criterion.

Yi et al. (2006) determined the constituents to be included in the harmonic analysis using the Lomb–Scargle periodogram analysis with a global optimization method of least squares and an interval search algorithm based on Mautz's (2002) methodology. However, depending on the uneven sampling characteristics of the data, this solution has some

disadvantages. Using simulated altimeter crossover data, Yi et al. (2006) showed that the root sum of squared vector differences in a single satellite crossover mission (TOPEX/Poseidon or Jason) is greater than that corresponding to a dual satellite crossover mission (TOPEX/Poseidon or Jason, ERS2). Yi et al. (2006) also found that the tidal constituents K_2 and Q_1 could not be identified and, in some cases, S_2, N_2, and P_1 also could not be successfully identified.

To decide which altimetry and tide gauge (with missing observations) data series could be used to calculate the harmonic constants of the eight aforementioned tidal constituents, a simulated series was generated for each altimeter crossover point and tide gauge position with missing data. In all cases, the simulated series maintained the intervals between observations.

In tide gauge records, oceanic signals with periods longer than the wave are found in addition to the tide signal. To build the simulated series, the sea-level observations from a tide gauge station were used. For this, the observations from Arturo Prat Base tide gauge were selected because they have the greatest series length (Table 1). The harmonic constants corresponding to the eight selected constituents for each simulated series were calculated and compared with those obtained from the entire series of Arturo Prat Base. If any constituent of the simulated series had a root mean square (RMS) misfit (Equation (2)) of >1.5 cm, then the original series was rejected and not used in the comparison:

$$\mathrm{RMS}_{\mathrm{misfit}} = \left(\frac{[H_o \cos(g_o) - H_s \cos(g_s)]^2 + [H_o \sin(g_o) - H_s \sin(g_s)]^2}{2} \right)^{1/2} \tag{2}$$

where H_o and g_o are respectively the amplitude and Greenwich epoch of the constituent of the Arturo Prat Base full series, and H_s and g_s are respectively the amplitude and Greenwich epoch of the constituent of the simulated series. The maximum value of 1.5 cm arises by considering that the eight constituents in phase would produce an error of 12 cm, coincident with the RMS misfit calculated between observed and prediction values for the entire set of Arturo Prat Base observations.

According to the Rayleigh criterion, for tide gauge short-length series, where it is not possible to separate the required constituents, the methodology proposed by Godin (1972) was followed to decontaminate the harmonic constants included in the analysis and to infer contaminant harmonic constants at close frequencies. This method uses amplitude ratios and epoch differences between contaminated and inferred harmonic constants at a nearby location with a reliable series of more than one year's length.

3.2. Misfits

The amplitudes and epochs obtained from the harmonic analysis of selected series of tide gauges and satellite altimeters were compared with the corresponding values obtained from the 12 tide models. The constituents Q_1, O_1, P_1, K_1, N_2, M_2, S_2, and K_2, which constitute the common set provided by the selected models (Table 2), were used for the comparison.

To quantify the constituent misfit between each model and the corresponding observational data, the RMS misfit was calculated using the following equation:

$$\mathrm{RMS}_{\mathrm{misfit}} = \left(\frac{1}{2N} \sum_{N} [H_1 \cos(g_1) - H_2 \cos(g_2)]^2 + [H_1 \sin(g_1) - H_2 \sin(g_2)]^2 \right)^{1/2} \tag{3}$$

where N is the number of observational data series, H_1 and g_1 are respectively the amplitude and Greenwich epoch corresponding to observational data, and H_2 and g_2 are respectively the amplitude and Greenwich epoch provided by the models for the same tidal constituent.

To quantify the performance of each model, the root sum square (RSS) was obtained from the RMS misfit

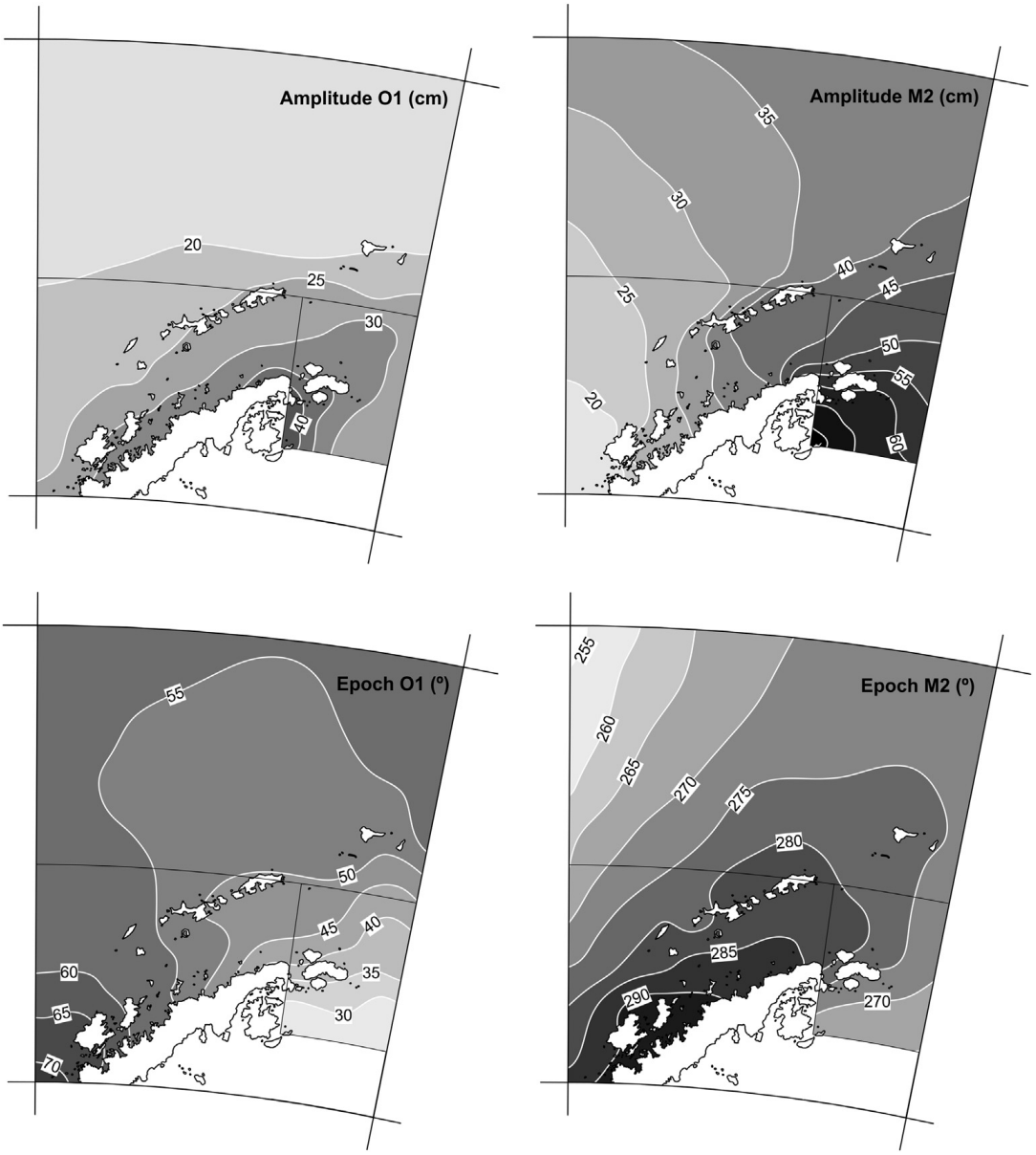

Fig. 2. (Upper) O_1 and M_2 isoamplitude charts. (Lower) Cotidal charts of the same constituents.

of the selected tidal constituents using the following equation:

$$\mathrm{RSS} = \sqrt{\sum_{j=1}^{M} \mathrm{RMS}_j^2}$$

where M is the number of constituents.

4. Results

4.1. Harmonic analysis

Using the described methodology, it was found that the constituents Q_1, O_1, P_1, K_1, N_2, M_2, S_2, and K_2 could be successfully extracted from 232 of the 293 original altimeter data series. The remaining data series did not have the required length and/or an adequate distribution of the missing data to be able to infer all harmonic constants.

For the tide gauge series, according to the Rayleigh criterion, 17 of the 20 tidal series available were too short to separate the eight required constituents (Table 1). For these 17 series, the methodology developed by Godin (1972) was followed to decontaminate the harmonic constants included in the analysis and to infer contaminant harmonic constants.

To obtain a comprehensive view of the behavior of each harmonic constant in the study area and to detect

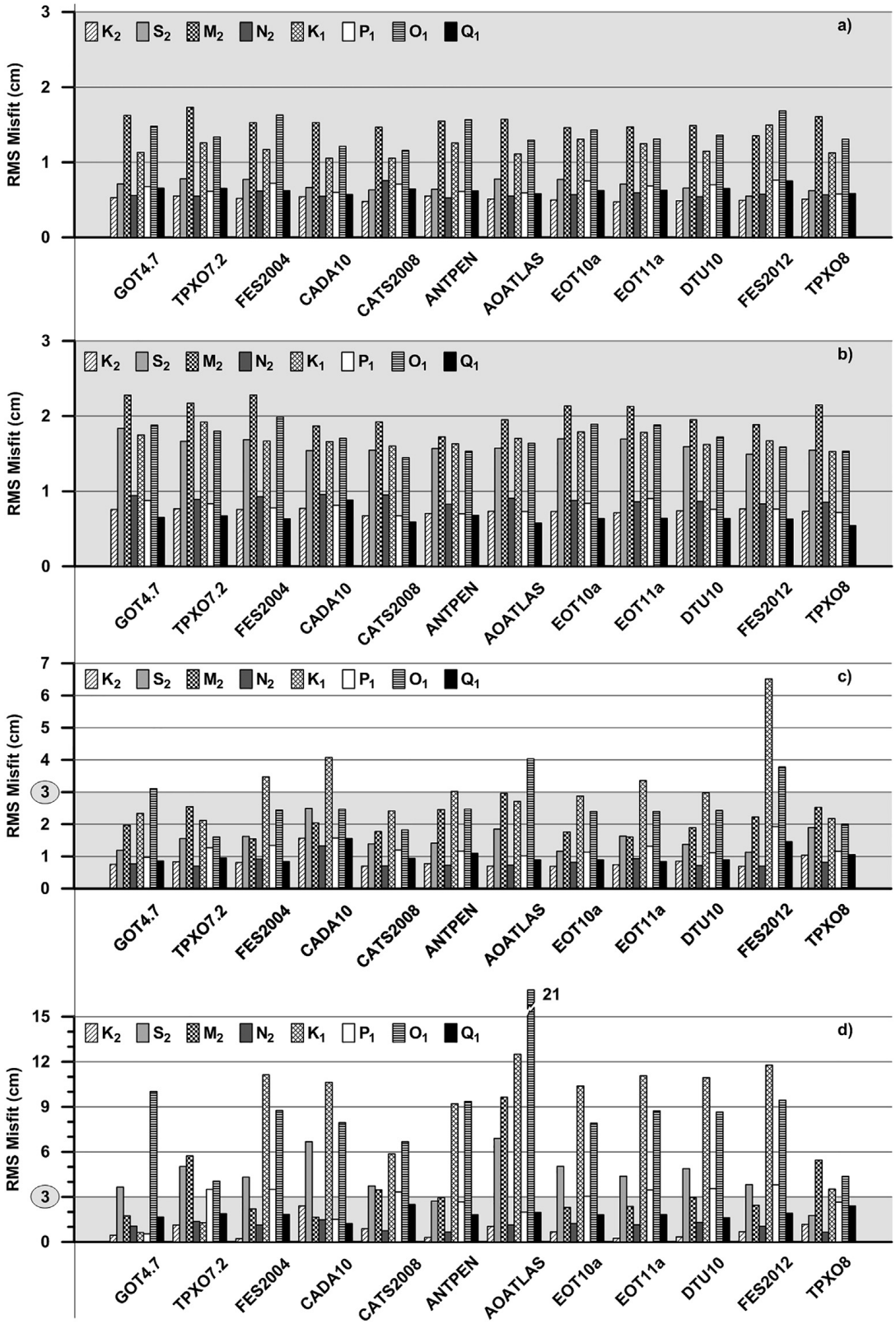

Fig. 3. Comparison of the RMS misfit obtained for each model and for each constituent for Zones I (a), II (b), III (c), and for Matienzo Base (d). The gray area denotes 3 cm of RMS misfit.

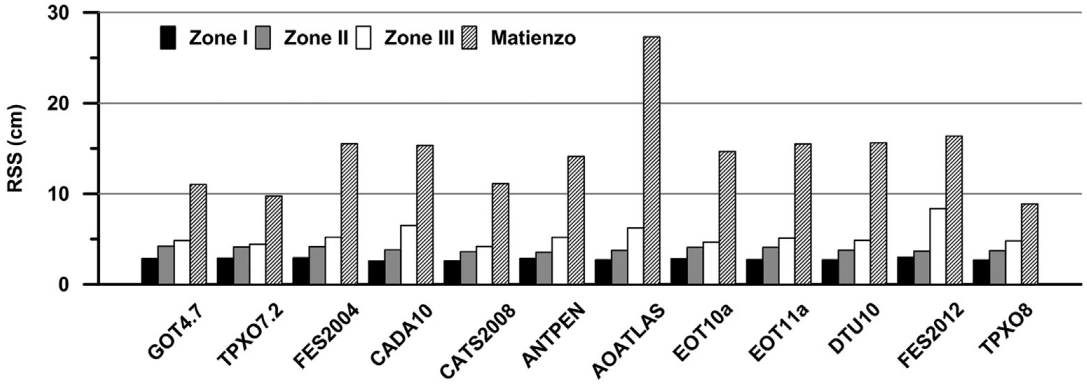

Fig. 4. Comparison of the RSS values obtained for all zones and each model.

any significant errors in the harmonic analysis, the isoamplitude and cotidal charts of all constituents were calculated. For the sake of brevity, cotidal and isoamplitude charts of only the most important semidiurnal and diurnal constituents, M_2 and O_1, are shown in Fig. 2.

Isoamplitude charts of all constituents reveal that the eastern sector of the study area presents the highest amplitudes of the studied constituents and that the amplitudes decrease in value northward. At the northern tip of the west coast of the Antarctic Peninsula, the M_2 (and the S_2, not shown) amplitude decreases southward, whereas the O_1 (and the K_1, not shown) amplitude remains practically constant. This explains the spatial variation in the tide regime calculated following Defant (1960), which is mixed, mainly semidiurnal type throughout most of the study area, and mixed, mainly diurnal type in the southwestern part of the study area.

The cotidal chart shows the M_2 constituent approaching from the northwest and in the southeast hugging the study area, completing its phase variation in 1.55 h. In contrast, O_1 travels from the southeast surrounding the study area, taking 3.80 h to reach the southwest.

4.2. Comparison of harmonic constants from observational data and tide models

It is possible that the RMS misfit depends strongly on the tidal range of the region considered. In these cases, the larger the tidal range, the larger the expected

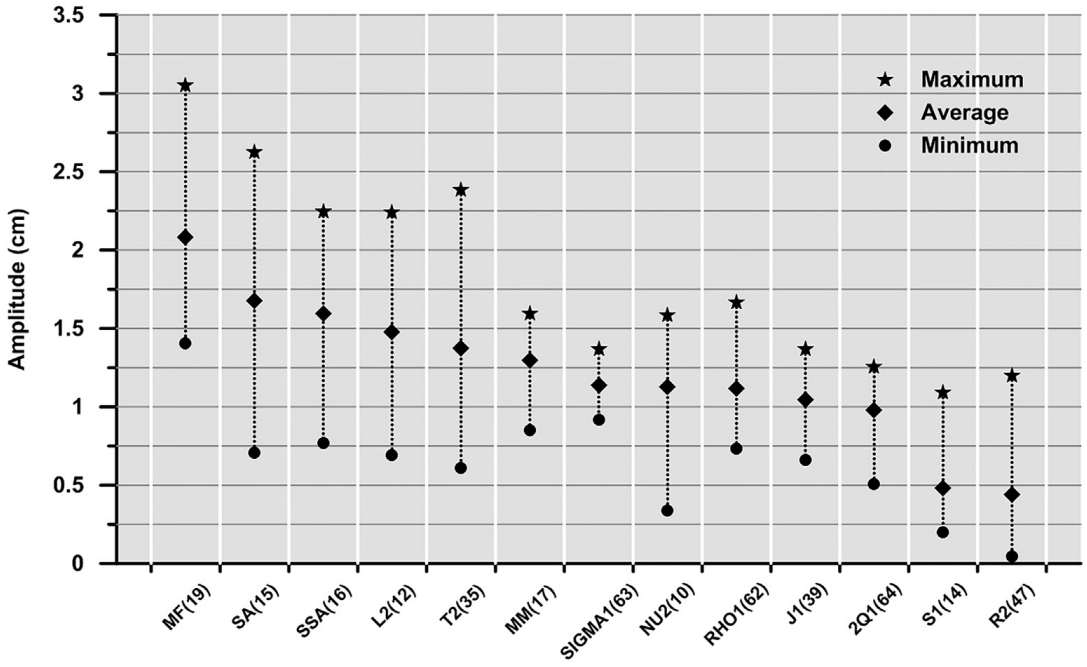

Fig. 5. Maximum, minimum, and average amplitudes for the tidal constituents (other than the eight common constituents used for the model comparisons) with (maximum) amplitudes greater than 1 cm.

RMS misfit. Moreover, in general, tide models used to detide SSH are more accurate in deep water than near the coast or in areas where there are few altimetry data, because of the presence of ice covering the water surface. These characteristics affect the models' performance and also influence the results of RMS misfit and RSS.

To discover the highest tidal range in the study area, which is not fully covered by tide tables (SHN, 2012), 20 years of tide predictions were made. The harmonic constants of the eight common constituents obtained from the harmonic analyses were used for locations in areas of higher or lower tidal range as identified by the isoamplitude charts. From this, it was found that the astronomical tidal range variation for the study area is about 217 cm. Then, to obtain a more representative RMS misfit and RSS, the study area was divided into three zones (Fig. 1) with similar maximum tidal amplitude variations and different physical characteristics (depth, land, continental shelf, and ice-covered surface).

Zone I, located to the north of the South Shetland Islands (north of 62°S), has a 90-cm maximum tidal amplitude variation, great depths of around 3300 m, and little presence of land. Zone II, located south of 62°S and west of the Antarctic Peninsula, has a 74-cm maximum tidal amplitude variation. Most of the Antarctic bases are located in Zone II. This zone is characterized by shallower depths than are found in Zone I, and contains a narrow continental shelf with greater depths close to the coast than are observed in Zone III. Zone III is located between 62°S and 64.3°S, and east of 58.5°W, presenting a 105-cm maximum tidal amplitude variation. Zone III, characterized by the shallowest depths among the three zones, has a continental shelf with a gentle slope and therefore shows the greatest recorded tidal amplitudes. Zone III has more floating ice than either of the other two zones, and consequently this zone has the lowest number of available altimetry data. Because there are insufficient satellite altimetry observations between Matienzo Base (64.9761°S, 60.0683°W) and the closest zone, this station was analyzed separately. Moreover, the tidal range of Matienzo Base is the highest in the entire study area, and would increase the extreme tidal amplitude variation of Zone III from 105 to 138 cm if it were included in this zone.

Fig. 3 shows, for each zone, the RMS misfit calculated between model results and the eight common constituents. For Zone I and all models, the RMS misfits for the most important semidiurnal and diurnal constituents, M_2 and O_1, vary between 1.3 and 1.7 cm and 1.2 and 1.7 cm, respectively. K_1 is less than 1.6 cm, whereas the rest of the constituents yield RMS misfits less than 0.8 cm. The RMS misfits for M_2, S_2, O_1, and K_1 vary between 1.5 and 2.3 cm for Zone II, and are less than or equal to 1.0 cm for the other constituents. The RMS misfits for Zone III are less than 4.1 cm, except for K_1 which yields 6.5 cm for the FES2012 model. Matienzo Base has the largest variations in the RMS misfit. M_2 and O_1 RMS misfits for Matienzo Base vary between 1.7 and 10.0 cm, except for the AOATLAS O_1 constituent at 21.0 cm K_1 and S_2 follow in importance, ranging from 0.6 to 12.5 cm and from 1.8 to 6.9 cm, respectively. RMS misfits for the rest of the constituents are less than 3.9 cm.

Fig. 4 shows the calculated RSS for all zones and models. RSS values are less than or equal to 3.0, 4.2, and 8.4 cm for Zones I, II, and III, respectively. For Matienzo Base, the lowest RSS corresponds to the TPXO8 model at 8.9 cm, leaving the remaining values between 9.8 and 16.4 cm, except for the AOATLAS model, which reaches 27.3 cm.

4.3. Major tidal constituents for the study area

Harmonic analyses were performed to verify the relative importance of the common tidal constituents provided by the selected models. These analyses were made with the longest time series constructed from the altimeter cross-tracks and with tide gauge coastal observations from Prat, Esperanza, and Brown bases. These bases were selected because they have the longest measurement periods (Table 1). The 123 constituents used by D'Onofrio et al. (2012) were used.

Although not all selected tide models use the same constituents, the constituents that are common to all models (O_1, K_1, P_1, Q_1, M_2, S_2, N_2, and K_2) have the largest amplitudes in the harmonic analysis conducted. The maximum, minimum, and average values of amplitudes of constituents that follow in importance after the eight common tidal constituents, and which have amplitudes greater than 1 cm, are shown in Fig. 5. The 13 constituents shown have amplitudes less than 3.1 cm.

5. Discussion and conclusions

The comparisons made in this work enable assessment of the performance of the models in areas with similar maximum tidal amplitude variations and different physical characteristics (depth, land, continental shelf, and ice-covered surface).

Zone I has the most comprehensive series of recorded altimetry data on account of the scarcity of both land and floating ice compared with the other zones. This means that a larger number of heights are available to be assimilated by the models, and the greater depths in this zone improve the models' performances. These characteristics provide this zone with the lowest RMS misfit results of the entire study area, less than 1.7 cm, and with no significant differences among the models. CATS2008 and CADA10 yield the lowest RSS for this zone, with a value of 2.6 cm, and the rest of the models present values of up to 3.0 cm.

Zone II has the most extensive tide gauge data, as most of the Antarctic bases are located on the western coast of the Antarctic Peninsula and the South Shetland Islands. RMS misfit values for this zone are less than 2.3 cm, with no significant differences among the models. Although Zone II has a significant number of coastal observations, the RSS values obtained in this zone are higher than those in Zone I. This difference may be caused by more land and floating ice in this zone. ANTPEN04.01 is the tide model with the lowest RSS in Zone II (3.5 cm), and the rest of the models show values of up to 4.2 cm. The better performance of the forward model ANTPEN04.01 in this zone may be because this model is particularly suited for studies of tidal heights and flows in narrow passages around the peninsula, the coastal islands, and other islands of Bransfield Strait (http://www.esr.org/polar_tide_models/Model_AntPen0401.html).

Zone III is characterized by the largest tidal amplitudes and the dominant presence of ice. There are fewer tide gauges in this zone compared with Zones I and II, and altimetry data are much scarcer. For these reasons, RMS misfit and RSS values for this zone are higher. The obtained RMS misfits are less than 4.1 cm, except for K_1 at 6.5 cm for the FES2012 model. Unlike Zones I and II, in Zone III there are significant differences in the RMS misfit values among the analyzed models. For all models, RSS values from Zone III are the largest, and in some models the values from Zone III are double those obtained for Zones I and II. This is consistent with the described characteristics of Zone III. The lowest RSS belongs to the CATS2008 model (4.2 cm). Carrère et al. (2012) argue that the degradation of FES2012 compared with FES2004 in the Southern Ocean is likely due to a lack of assimilated data (currently, no data are assimilated). These results agree with the inferior performance of FES2012 compared with FES2004 in Zone III, but they are not consistent with the similar RSS values shown by these two models in zones I and II.

There is no single model that has a superior performance in all zones, and the present results therefore allow the model with the best performance to be selected depending on the zone of interest. The results also show the need for further sea-level measurements in Zone III, as the models yield the greatest RMS misfit and RSS values in this zone.

Matienzo Base presents RMS misfit and RSS values that are generally more than twice those obtained for the rest of the study area. Although the largest amplitudes of the selected constituents were generally found in Matienzo Base, these amplitudes do not entirely justify the values of RMS misfit and RSS found. A more likely cause for these high values is the lack of nearby altimetry and tide gauge data to be assimilated by the different models. Before 1995, the nunatak where Matienzo Base is located was surrounded by the Larsen Ice Shelf. This shelf began to disintegrate in the northern boundary between 1995 and 2002 and subsequently in the southern boundary. Taken together, this shelf and the permanent presence of floating ice explain the lack of altimetry data around Matienzo Base. The smallest RSS values for Matienzo Base correspond to models TPXO8 (8.8 cm) and TPXO7.2 (9.8 cm), for which the harmonic constants of this station, determined by D'Onofrio et al. (2003), were assimilated in both solutions.

Fig. 5 shows that the most important constituent among the long-period constituents is M_f, with an average value of 2.1 cm. This constituent is included in the global models TPXO7.2, TPXO8, FES2004, FES2012, EOT10a, and EOT11a, and in the regional models CATS2008 and CADA00.10. The constituents that follow in importance are S_a and S_{sa}, with average values of 1.7 and 1.6 cm, respectively; these two constituents are not included in any of the models, except for FES2012, which includes S_{sa}. The mean amplitudes of the $SIGMA_1$, RHO_1, $2Q_1$, and J_1 tidal constituents are around 1.0 cm and are not taken into account by the utilized models, except FES2012, which includes the J_1 constituent. The tide models GOT4.7, EOT10a, EOT11a, FES2004, FES2012, and DTU10 include the S_1 constituent, with an average amplitude 0.5 cm; although this value is not significant in the present study area, it could be important in other regions covered by these models. L_2 and T_2 stand out between semidiurnal constituents with average amplitudes of 1.5 and 1.4 cm, respectively. FES2012 is the only model that takes into account the L_2 and T_2 constituents. Shallow-water constituents are not found for amplitudes greater than 1 cm, which is consistent with the selection of constituents for the regional

models of Antarctica. This identification of the most important constituents for the study area should represent a valuable contribution to the field of tide modeling.

Yi et al. (2006) compared the results from models NAO.99b, TPXO6.2, and CATS02.01 with harmonic constants of 13 coastal stations in Antarctica, 10 of which are located in Zone II, and obtained RSS values of 19.54, 18.78, and 18.50 cm, respectively. In the present study, RSS values for models TPXO8 and CATS2008 (which are updated versions of models TPXO6.2 and CATS02.01, respectively) were calculated for the coastal stations located in Zone II, and yielded values of 6.3 and 6.7 cm, respectively. Although these results do not correspond to the same stations used by Yi et al. (2006), the results presented here suggest an improvement in the models. However, the performance of the models could be further improved in future work, particularly in the vicinities of Zone III and Matienzo Base, by incorporating satellite and/or tide gauge measurements as they become available.

Acknowledgments

This research comprises part of the 20020100100840 UBACyT 2011–2014 Science and Technological Division, University of Buenos Aires (UBACYT) Project and is a contribution to the PID-DEF 42/10 projects (Ministry of Defense, Naval Hydrographic Service).

References

Bendat, J.S., Piersol, A.G., 1971. Random Data: Analysis and Measurement Procedures. Wiley-Interscience, New York.

Bianchi, A.A., Bianucci, L., Piola, A.R., Pino, D.R., Schloss, I., Poisson, A., Balestrini, C.F., 2005. Vertical stratification and air–sea CO_2 fluxes in the Patagonian shelf. J. Geophys. Res. 110, C07003. http://dx.doi.org/10.1029/2004JC002488.

Birkett, C., Reynolds, B., Beckley, B., Doorn, B., 2011. From research to operations: the USDA global reservoir and lake monitor. In: Vignudelli, S., Kostianoy, A., Cipollini, P., Benveniste, J. (Eds.), Coastal Altimetry. Springer, Berlin, pp. 19–50.

Brunt, K.M., King, M.A., Fricker, H.A., MacAyeal, D.R., 2010. Flow of the Ross ice shelf, Antarctica, is modulated by the ocean tide. J. Glaciol. 56 (195), 157–161.

Carrère, L., Lyard, F., Cancet, M., Guillot, A., Roblou, L., 2012. FES2012: a new global tidal model taking advantage of nearly 20 years of altimetry. In: Proceedings of Meeting "20 Years of Altimetry", Venice.

Cartwright, D.E., 1985. Tidal prediction and modern time scales. Int. Hydrographic Rev. LXII (1), 127–138.

Chelton, D.B., Ries, B.J., Haines, B.J., Fu, L.L., Callahan, P.S., 2001. Satellite altimetry. In: Fu, L.L., Cazenave, A. (Eds.), Satellite Altimetry and Earth Sciences. International Geophysics Series, New York, pp. 1–126.

Chen, G., Lin, H., 2000. The effect of temporal aliasing in satellite altimetry. Photogramm. Eng. Rem. Sens. 66 (5), 639–644.

Cheng, Y., Andersen, O., 2011. Multimission empirical ocean tide modeling for shallow waters and polar seas. J. Geophys. Res. 116, C11001. http://dx.doi.org/10.1029/2011JC007172.

Defant, A., 1960. The harmonic analysis of tidal observations. In: Physical Oceanography. Pergamon Press, Oxford, pp. 299–319.

D'Onofrio, E., Dragani, W., Speroni, J., Fiore, M., 2003. Propagation and amplification of tide at the northeastern coast of the Antarctic Peninsula: an observational study. Polar Geosci. 16, 53–60.

D'Onofrio, E., Oreiro, F., Fiore, M., 2012. Simplified empirical astronomical tide model—an application for the Río de la Plata estuary. Comput. Geosci. 44, 196–202.

Dragani, W.C., D'Onofrio, E.E., Speroni, J.O., Fiore, M.E., Borjas, R., 2005. A numerical study of the ocean circulation around the northern Antarctic Peninsula: barotropic response to tidal forcing. Polar Geosci. 18, 83–100.

Egbert, G.D., Ray, R.D., 2000. Significant dissipation of tidal energy in the deep ocean inferred from satellite altimeter data. Nature 405, 775–778.

Egbert, G.D., Ray, R.D., 2001. Estimates of M_2 tidal energy dissipation from TOPEX Poseidon altimeter data. J. Geophys. Res. 106, 22475–22502.

Egbert, G.D., Erofeeva, S.Y., 2002. Efficient inverse modeling of barotropic ocean tides. J. Atmos. Oceanic Technol. 19, 183–204.

Foldvik, A., Middleton, J.H., Foster, T.D., 1990. The tides of the southern Weddell Sea. Deep-Sea Res. 37, 1345–1362.

Godin, G., 1972. The Analysis of Tides. University of Toronto Press, Toronto.

King, M.A., Padman, L., Nicholls, K., Clarke, P.J., Gudmundsson, G.H., Kulessa, B., Shepherd, A., 2011. Ocean tides in the Weddell Sea: new observations on the Filchner-Ronne and Larsen C ice shelves and model validation. J. Geophys. Res. 116, C06006. http://dx.doi.org/10.1029/2011JC006949.

Ledwell, J.L., Montgomery, E.T., Polzin, K.L., St. Laurent, L.C., Schmitt, R.W., Toole, J.M., 2000. Evidence for enhanced mixing over rough topography in the abyssal ocean. Nature 403, 179–182.

Legrésy, B., Wendt, A., Tabacco, I., Remy, F., Dietrich, R., 2004. Influence of tides and tidal current on Mertz Glacier, Antarctica. J. Glaciol. 50, 427–435.

Levine, M.D., Padman, L., Muench, R.D., Morison, J.H., 1997. Internal waves and tides in the western Weddell Sea: observations from Ice Station Weddell. J. Geophys. Res. 102, 1073–1089.

Lutjeharms, J.R.E., Stavropolous, C.C., Koltermann, K.P., 1985. Tidal measurements along the Antarctic coastline. In: Jacobs, S.S. (Ed.), Oceanology of the Antarctic Continental Shelf, Antarctic Research Series, vol. 43. AGU, Washington, D.C, pp. 273–289.

Lyard, F., Lefevre, F., Letellier, T., Francis, O., 2006. Modeling the global ocean tides: modern insights from FES2004. Ocean Dyn. 56 (5–6), 394–415.

Mautz, R., 2002. Solving nonlinear adjustment problems by global optimization. Bollet. Geode. Scien. Affini. 64, 123–134.

Munk, W., Cartwright, D.E., 1966. Tidal spectroscopy and prediction. Phil. Trans. R. Soc. Lond. A 259 (1105), 533–581.

Munk, W.H., Wunsch, C., 1998. Abyssal recipes II: energetics of tidal and wind mixing. Deep-Sea Res. 45, 1977–2010.

Padman, L., Fricker, H.A., Coleman, R., King, M., 2001. Improving models of Antarctic ice shelf tides through data assimilation. In:

European Geophysical Society Meeting, Nice, France, April, Poster.

Padman, L., Fricker, H.A., Coleman, R., Howard, S., Erofeeva, S., 2002. A new tidal model for the Antarctic ice shelves and seas. Ann. Glaciol. 34, 247–254.

Padman, L., Erofeeva, S.Y., Fricker, H.A., 2008. Improving Antarctic tide models by assimilation of ICES at laser altimetry over ice shelves. Geophys. Res. Lett. 35, L22504. http://dx.doi.org/10.1029/2008GL035592.

Pedley, M., Paren, J.G., Potter, J.R., 1986. The tidal spectrum underneath Antarctic ice shelves. J. Geophys. Res. 91, 13001–13009.

Polzin, K.L., Toole, J.M., Ledwell, J.R., Schmitt, R.W., 1997. Spatial variability of turbulent mixing in the abyssal ocean. Science 276, 93–96.

Pugh, D.T., 1987. Tides, Surges and Mean Sea-Level. John Wiley and Sons Ltd., Chichester.

Pugh, D.T., 2004. Changing Sea Levels: Effects of Tides, Weather and Climate. Cambridge University Press, U.K.

Ray, R.D., 1999. A Global Ocean Tide Model from TOPEX/POSEIDON Altimetry: GOT99.2. Rep. NASA/M-1999–209478Rep. Goddard Space Flight Center, Greenbelt, Md, p. 58.

Romero, S.I., Piola, A.R., Charo, M., García, C.A.E., 2006. Chlorophyll*a* variability off Patagonia based on SeaWiFS data. J. Geophys. Res. 111, C05021. http://dx.doi.org/10.1029/2005JC003244.

Saraceno, M., D'Onofrio, E.E., Fiore, M.E., Grismeyer, W.H., 2010. Tide model comparison over the Southwestern Atlantic Shelf. Cont. Shelf Res. 30, 1865–1875.

Savcenko, R., Bosch, W., 2010. EOT10a––Empirical Ocean Tide Model from Multi-mission Satellite Altimetry. Deutsches Geodätisches Forschungsinstitut (DGFI), München. Available for download at: ftp://ftp.dgfi.badw.de/pub/EOT10a/.

Savcenko, R., Bosch, W., 2011. EOT11a––a new tide model from Multi-Mission Altimetry. In: OSTST Meeting, October 19–21, San Diego.

Schureman, P., 1988. Manual of Harmonic Analysis and Prediction of Tides. U.S. Department of Commerce, Coast and Geodetic Survey. Special Publication No. 98.

SHN, 2012. Tablas de Marea para la Antártida Octubre 2011–Diciembre 2012. Departamento Oceanografía, Servicio de Hidrografía Naval, Ministerio de Defensa, Buenos Aires, Argentina.

Smith, A.J.E., Ambrosius, B.A.C., Wakker, K.F., 2000. Ocean tides from T/P, ERS-1, and GEOSAT altimetry. J. Geodesy. 74, 399–413.

Yi, Y., Matsumoto, K., Shuma, C.K., Wanga, Y., Mautz, R., 2006. Advances in Southern Ocean tide modeling. J. Geodyn. 41, 128–132.